J Solid State Electrochem (2010) 14:531–542
DOI 10.1007/s10008-008-0663-7

ORIGINAL PAPER

Characterisation of the electrochemical redox behaviour of Pt electrodes by potentiodynamic electrochemical impedance spectroscopy

G. A. Ragoisha · N. P. Osipovich · A. S. Bondarenko · J. Zhang · S. Kocha · A. Iiyama

Received: 2 June 2008 / Revised: 28 July 2008 / Accepted: 26 August 2008 / Published online: 12 September 2008

Abstract Multi-frequency ac responses of Pt in aqueous solutions of sulphuric and perchloric acids have been characterised in cycles of Pt oxide anodic formation and cathodic reduction as functions of electrode potential, using the two orders frequency range below 1 kHz, where the double layer responded jointly with Faradaic processes. The potentiodynamic impedance spectra were fitted to an equivalent circuit, which contained double-layer capacitance in parallel with charge transfer resistance, R, and constant phase element (CPE). Double-layer capacitance has shown minima (20–25 μF cm^{-2} in 0.5 M H_2SO_4 and 25–35 μF cm^{-2} in 1 M $HClO_4$) in the double-layer region and more than twofold increase in the platinum oxidation region. R^{-1} and CPE have shown maxima in the regions of platinum oxidation and reduction. Potentiodynamic curves of raw impedance data were also self-descriptive in monitoring platinum oxidation and reduction in both solutions and in presence of chloride.

Presented at the 5th Baltic Conference on Electrochemistry, Tartu, 30 April–3 May 2008.

G. A. Ragoisha (✉) · N. P. Osipovich
Physico-Chemical Research Institute, Belarusian State University, Minsk 20050, Belarus
e-mail: ragoisha@yahoo.com
URL: http://www.abc.chemistry.bsu.by/vi/

A. S. Bondarenko
University of Twente,
Enschede, The Netherlands

J. Zhang · S. Kocha · A. Iiyama
Fuel Cell Laboratory, Nissan Research Center,
Kanagawa 237-8523, Japan

Keywords Platinum · Anodic oxide · Potentiodynamic electrochemical impedance spectroscopy · Double-layer capacitance

Introduction

Platinum anodic oxidation is an extensively reviewed but still disputable subject [1–13]. Mechanisms of the oxide formation have been reconsidered lately [6–9], and there is no accord among the researches even on such a basic issue as the product of Pt anodic oxidation at the initial stages of the oxide film growth. Experimental data, such as the electrode mass changes measured using quartz crystal microbalance in the anodic scan, have been considered to support either anhydrous oxide [6, 7] or hydroxide [8] formation. Recent discussions on the mechanisms of platinum oxidation show that the object still lacks sensitive and informative technique for in situ comprehensive characterisation of the variable electrochemical interface at the initial stages of oxide growth and reduction.

Nowadays, the interest in the mechanisms of platinum oxide formation, reduction and dissolution has been stimulated greatly by the fuel cell demand for durable catalysts with low Pt content [14–20]. Pt is more resistant to anodic dissolution than other platinum group metals in the potential range of oxide growth [21]. However, the dissolution rate is strongly dependent on the potential profile [16] and can be accelerated up to four orders of magnitude by the potential cycling [18]. The dissolution rate is sensitive to impurities, e.g. chloride has been found to accelerate Pt dissolution even at very low concentration, as low as 10 ppm [22].

The major problems with characterisation of platinum anodic oxidation come from limitations of non-stationary

techniques. Though surface science has effective techniques available for atomic layers characterisation ex situ, electrochemists still have to use mainly cyclic voltammetry (CV) for considering the electrode surface changes under potentiodynamic conditions. Electric current is a convenient source of information about the electrode status variation in the potential scan, and almost every publication on anodic oxidation of Pt contains a voltammetric profile. CV is used traditionally as a signature of Pt electrode surface status mainly due to the characteristic peaks of hydrogen underpotential deposition (upd). However, CV is not self-descriptive for Pt in the potential regions above H upd. The potentiodynamic profile of polycrystalline Pt electrode in sulphuric acid is flat in the double-layer region where Pt can adsorb sulphate [23, 24].

Limitation of CV in the double-layer and oxide formation regions is probably a reason of the widespread belief in the double-layer capacitance (C_{dl}) invariability on the potential. As for the border of the double-layer and the H upd region, Pajkossy and Kolb [25, 26] found recently a sharp C_{dl} peak in that region using the common (stationary) electrochemical impedance spectroscopy (EIS).

EIS is a useful tool for platinum–electrolyte solution interface characterisation, especially in those potential ranges where dc current response is not self-descriptive. However, the common EIS was designed to work with stationary systems. Its application to platinum anodic oxide characterisation normally requires keeping first the electrode in the Pt oxidation range to attain a quasi-stationary state and then going down to the desired potential for the frequency response measurement [27]. The electrode status at a given potential in that protocol of the frequency response measurement should be obviously different from the one attained in the cyclic potential scan.

The ac voltammetry overcomes hindrance of the system's non-stationarity, but it lacks one of the major characteristics of the ac response—the frequency response, which is the basic feature of EIS. The potentiodynamic impedance spectrum can be compiled from many ac voltammograms recorded at different frequencies [28], but that way of obtaining the potentiodynamic frequency response is critically dependent on exact repetition of the processes trajectory in space of many variables.

Potentiodynamic electrochemical impedance spectroscopy (PDEIS) [29–33] obtains the information on ac responses in different frequencies in a single staircase potential scan. The steps of the potential staircase are typically from 1 to 2 mV, so the staircase is close to a continuous slope of the voltammetric scan, and the ac probing is realised by a sequence of low-amplitude wavelets. The responses in different frequencies are extracted from different regions on the time scale, unlike the case with Fourier transform impedance techniques [34] where the whole multi-frequency probing signal is treated as a source of information on each frequency. The latter difference is important for providing better separability of the multi-frequency response with PDEIS in non-stationary system examination where the ac responses are inevitably nonlinearly distorted even at low amplitudes of the probing signal.

It is important to note a difference between potentiodynamic and potentiostatic techniques. Being a potentiodynamic technique, PDEIS not only monitors dependences of ac electrochemical responses on electrode potential but also gives information about process trajectory in the potential scan. Only for perfectly reversible systems, the processes paths can coincide in the forward and backward scans, whilst in general case, the system under investigation passes through different states in both directions of the scan, so the potentiodynamic response in PDEIS is dependent on the scan direction and rate [29]. Due to this peculiarity, which is also inherent to potentiodynamic voltammetry, the potentiodynamic techniques can monitor non-stationary processes that cannot be characterised by just recording the potential dependences of the same variables at stationary conditions. A well-known example is represented by objects with electrochemical adsorption, such as the cathodic underpotential deposition of a metal atomic layer and its subsequent stripping in the anodic scan. Cyclic voltammetry, which is a potentiodynamic technique, gives characteristic peaks of atomic layer underpotential deposition and dissolution, whilst no upd peak can be observed in stationary voltammetry, as the stationary current of electrochemical adsorption is equal to zero.

The idea of applying PDEIS to characterise the variable status of platinum electrode surface during the oxide formation and reduction was based on the preceding applications of this technique for investigation of the electrochemical deposition of metal atomic layers [29, 30, 35–37] and multilayers [38, 39]. The multi-frequency ac response has been shown to be both sensitive and selective to different interfacial process and structures. PDEIS combines the advantage of the 2D (amplitude and phase) signal in the potentiodynamic ac probing with the opportunity of frequency response analysis, which normally is a feature of stationary techniques. The 2D nature of the ac response is important for the separation of constituent responses. Both the amplitude and the phase of the ac signal are affected strongly by adsorption and redox changes on the electrode surface. It is also important that the information about phases comes from the electrochemical experiment control on the time scale, and the timescale of the response can be tackled much more accurately than the amplitude in the electrochemical experiment [30, 31]. Furthermore, the contributions of different interfacial objects in the ac response of the electrochemical interface depend differently on the frequency of the ac probing, and this allows their

separation in the PDEIS spectrum. In this paper, we show how this works on platinum in Pt|0.5 M H_2SO_4 and Pt|1 M $HClO_4$ systems in the potential regions of Pt surface redox transformations and also in the double-layer region where the electrode surface prepares for the oxidation, which takes place in the anodic scan at higher potential.

Experimental

Pt working electrodes (geometric surface area approximately 0.01 cm^2) were prepared by careful fusing of Pt wire (ChemPur) into glass capillaries. The Pt–glass–air three-phase boundary was controlled with optical microscope to avoid formation of microcavities. Before each series of experiments, the electrodes were etched with nitrohydrochloric acid, washed with water, flame-annealed and, after cooling in air, placed into the working solution (0.5 M H_2SO_4 or 1 M $HClO_4$ at room temperature, deaerated by Ar bubbling). Before using, electrodes were cycled within potential ranges of hydrogen upd and Pt oxidation to eliminate surface texturing features introduced by the annealing. After the cycling, the electrodes showed the typical voltammetric response of polycrystalline platinum (Fig. 1). The real surface area of the working electrodes was evaluated at this stage from cyclic voltammograms by the standard procedure of hydrogen adsorption current integration [40]. The double-layer capacitance and parameters of Faradaic impedance were normalised to the surface area in PDEIS data analysis.

The potential was controlled in a three-electrode cell (with a platinised Pt counter electrode) using the standard hydrogen electrode as a reference (Pt|H_2 in 0.5 M H_2SO_4 or 1 M $HClO_4$ matching the working electrolyte solution). The description of the PDEIS technique and data analysis is available elsewhere [29–33, 41]. The PDEIS virtual spectrometer combines the impedance spectra acquisition program which plots the frequency response variation in real time and the PDEIS spectra analyser routine. The built-in version of the analyser processes the whole PDEIS spectrum in a single run giving at the output the dependences of equivalent circuit parameters on the potential with information on goodness of fit and uncertainties for each parameter at each potential step in the spectrum. The version of the EIS Spectrum Analyser program which uses the same algorithms of fitting adapted for processing common (2D) EIS spectra is available on the Web as a freeware [42].

The PDEIS spectrum obtained in real time is a set of three 3D plots, which are formed by extending into 3D space (using electrode potential E as the additional variable) the common Nyquist plot and two Bode plots. Each of these 3D plots can be considered as an object formed by moving the corresponding 2D impedance spectrum along the E axis. The discreetness of the PDEIS spectrum along E axis was typically 2 mV. This was smaller than the amplitude of the ac probing, so the spectra and the dependences of parameters calculated from the spectra were quasi-continuous along the E axis. The probing ac amplitude was typically from 5 to 10 mV. These values were a kind of compromise to provide acceptable signal/noise ratio with minimal nonlinear distortions.

Ac frequencies were selected in the range between 10 Hz and 1 kHz. PI-50 potentiostat was used as actuator of the PDEIS virtual spectrometer. Typical number of frequencies in the spectra that were appropriate for accurate analysis of the frequency response was from 15 to 20, and such spectra were recorded at scan rates from approximately one to few millivolts per second. Low-frequency parts of spectra had to be omitted to allow faster scans. A relation between attainable scan rates and ac frequencies has been discussed in literature related to Fourier transform impedance technique [43].

The equivalent circuit which applies in the double-layer region and in the initial stages of platinum oxidation in cyclic scans is shown in Fig. 2 (the origin of this circuit is explained in the next section). The misfit between experimental data and this model was less then 10^{-4}, and in most cases, it was close to 10^{-5}. The lowest individual parameter uncertainty in the data fit to the model was obtained for C_{dl}

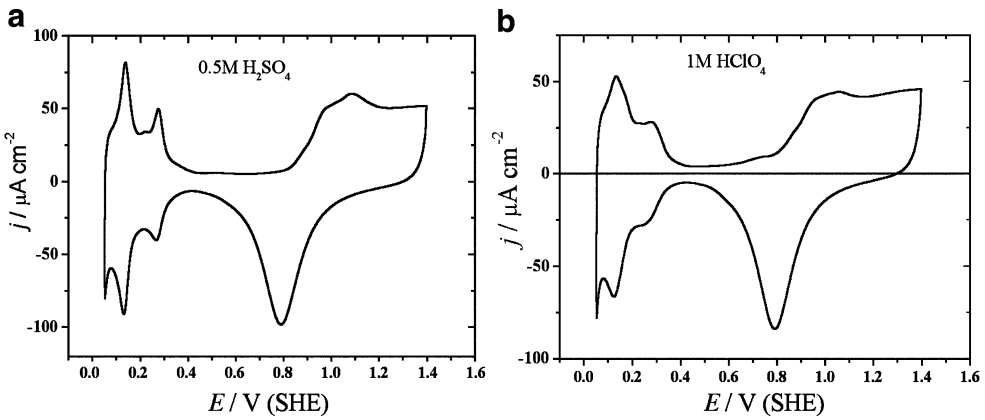

Fig. 1 Cyclic voltammograms of Pt electrode in 0.5 M H_2SO_4 (**a**) and 1 M $HClO_4$ (**b**) at 50 mV/s

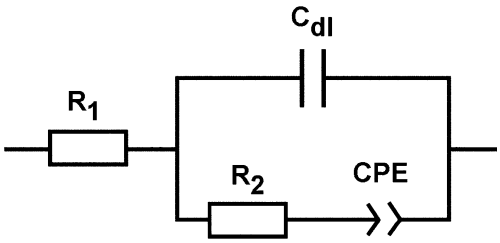

Fig. 2 Equivalent circuit

parameter (always within 1%), whilst the uncertainties of R_2 and constant phase element (CPE) were few times higher. The uncertainty of parameters is the characteristic supplementary to the goodness of fit, and it shows how each of the parameters is important to the model. The uncertainty within one or few percent corresponds to good appropriateness of the circuit element, and we observed very low noise in C_{dl} dependences on the potential, which were calculated from PDEIS spectra. The parameters of the Faradaic/adsorption branch also showed informative dependences on the potential, but with somewhat higher noise, which was due to the smaller contribution to the total ac response of the corresponding circuit elements. The element of the equivalent circuit R_1 represents mainly the solution resistance, which is not a function of the potential. Typical value of R_1 is 40 Ω. As the relative contribution of R_1 to the total ac response is small, minor variations of R_1, which can be observed in fitting are of the order of experimental error and therefore have no practical importance, unlike the variations of the other elements.

The choice of the frequency ranges was a compromise between the scan rate and the richness of spectrum content. We had to truncate the frequency response at few tens of Hertz to allow investigation of the dynamic features. Because of the limited frequency range, despite the reliable separation of the C_{dl} from the rest of the circuit, we were able to separate the branch in parallel to the C_{dl} only in the two elements, R_2 and CPE. Sulphate adsorption was probably too fast [44] to manifest elements of its own in the PDEIS spectra analysis in the tested frequency region. The double-layer capacitance did not show tendency of transforming into a CPE, unlike the case described in [28] where the impedance data were collected frequency by frequency from different ac voltammograms.

For easier visual perception of the graphical signatures formed by the multidimensional dependence of Pt ac response in the potential scan, PDEIS spectra were also recorded with fewer frequencies than required for frequency response analysis.

The real-time analysis of the multi-frequency ac response in PDEIS gives also the dc part of the response, in addition to the PDEIS spectrum. The dc voltammogram thus obtained is similar but not strictly equivalent to the classical analogue CV, as the algorithm of the digital probing in PDEIS does not integrate the whole dc charge. Therefore, we have presented in the next section only few samples of cyclic voltammograms obtained from the same scan with PDEIS spectrum. These digitally obtained voltammograms are helpful for comparing the potential ranges of the ac and dc responses, but they are not intended to be used for coulometric purposes in non-stationary processes characterisation.

Results and discussion

PDEIS spectra of Pt in 0.5 M H_2SO_4 and 1 M $HClO_4$

A potentiodynamic impedance spectrum is a 3D extension of a common impedance spectrum, which can be considered as a stack of many Nyquist plots or Bode plots recorded at different potentials in a staircase potential scan. The 3D object is formed by a common 2D spectrum moving in the direction perpendicular to the plain of the 2D plot. As the potential is the scanned variable, it is usually convenient to observe a thus formed 3D object in the orthogonal projection on a plain formed by the potential axis and one of the axes of the 2D plot, e.g. E and Im[Z] in the case of the extended Nyquist plot, as shown in Fig. 3. Each red line in this figure is a trajectory of one frequency point of the Nyquist plot in the forward scan which starts in the positive direction in Fig. 3a and in negative direction in Fig. 3b. The blue lines give the similar trajectories of points of equal frequency for the reverse scan. We will use also the black colour for the filling between the red lines and yellow colour for the filling between the blue lines in the PDEIS spectra representation.

PDEIS spectra of Pt in 0.5 M H_2SO_4 and 1 M $HClO_4$ have been found to show more complex and specific signatures of the potentiodynamic response than the cyclic voltammograms (Figs. 3, 4, 5, 6 and 7). Figure 3 shows the PDEIS spectra of Pt|0.5 M H_2SO_4 system in the cyclic scans started in different directions at 1.83 mV/s. Few examples of Nyquist plots from Fig. 3b are shown in Fig. 3c. The significant difference of the impedance spectra obtained at same potentials in the cathodic and anodic scans discloses the system irreversibility in different regions of potential. Figure 3d shows a potentiodynamic ac response just for two frequencies, but in wider potential range, which includes also H upd. We will use Fig. 3d to define peculiarities of Pt ac response in different potential regions.

1. In hydrogen upd region, Im[Z] is very low and shows two minima, thus disclosing the pseudo-capacitive origin of the corresponding peaks in the CV. This potential region will not be further analysed in this work.
2. Transition from H upd region to the double-layer region results in a strong increase in Im[Z].

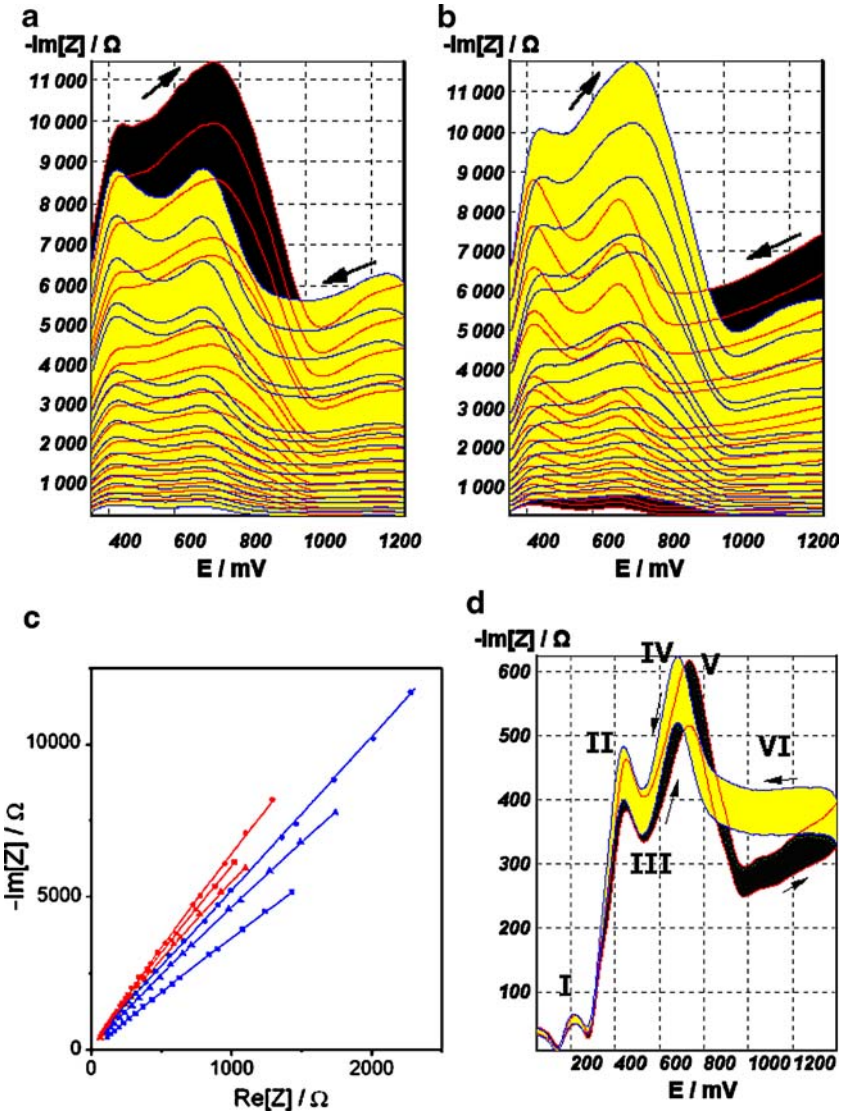

Fig. 3 PDEIS spectra of Pt in 0.5 M H_2SO_4 at **a**, **b** 1.83 mV/s [17 frequencies from 23.4 Hz to 439 Hz, cyclic scans were started from 0.35 V (**a**) and 1.3 V (**b**)]; **d** 40 mV/s (292 Hz and 351 Hz). Examples of Nyquist plots from **b** are shown in **c** for three potentials (700 mV, *circles*; 900 mV, *triangles*; 1,000 mV, *squares*). The curves in the Nyquist plot show data fit to the model. *Red symbols* and *lines* correspond to the forward scan, which was the cathodic scan in **b** and **c**; *blue symbols* and *lines* correspond to backward scans

3. The local minimum in Im[Z] in the double-layer region is characteristic to Pt|0.5 M H_2SO_4 system. At low scan rates, the minimum becomes less pronounced in the anodic scan, as shown in Fig. 3a,b. The local minimum in the double-layer region has been attributed to sulphate (bisulphate) adsorption. Figure 4a,c shows a clear distinction between Im[Z](E) dependences in sulphuric and perchloric acids. In the latter case, a single peak of Im[Z] is characteristic to the double-layer region. The spectra in Fig. 4 are shown overlaid on the digital CVs. Figure 4b,d shows also the ac phase potentiodynamic profiles (θ variation with the potential) for the same potential cycles as in Fig. 4a,c.
4. The increase in Im[Z] above 0.6 V is characteristic of Pt|0.5 M H_2SO_4, but not of Pt|1 M $HClO_4$ system.
5. The strong decrease in Im[Z] in the beginning of Pt oxidation in 0.5 M H_2SO_4 is accompanied by a peculiar hysteresis in the phase potentiodynamic profile (Fig. 4b). The Im[Z] decrease starts much earlier in perchloric acid. The hysteresis in the phase shift variation in the beginning of Pt oxidation is less pronounced in $HClO_4$.
6. The most distinctive feature of platinum anodic oxidation in the anodic scan is the phase shift minimum (Figs. 4b,d and 5) at 1.0 V. The left slope, which leads to the minimum of the phase shift, was found to be sensitive to electrode history.

Figure 6 shows the potentiodynamic profiles of Im[Z], Re[Z] and θ for the same systems as in Fig. 4, just with the addition of 10^{-4} chloride. Even at such a low concentration, chloride equalises the Im[Z] potentiodynamic profiles of Pt in sulphuric and perchloric acids and imposes much similarity into Re[Z] and θ potentiodynamic profiles. Figure 7 shows the similar potentiodynamic profiles for a greater number of frequencies, and the chloride affects them in a wide range of the potential.

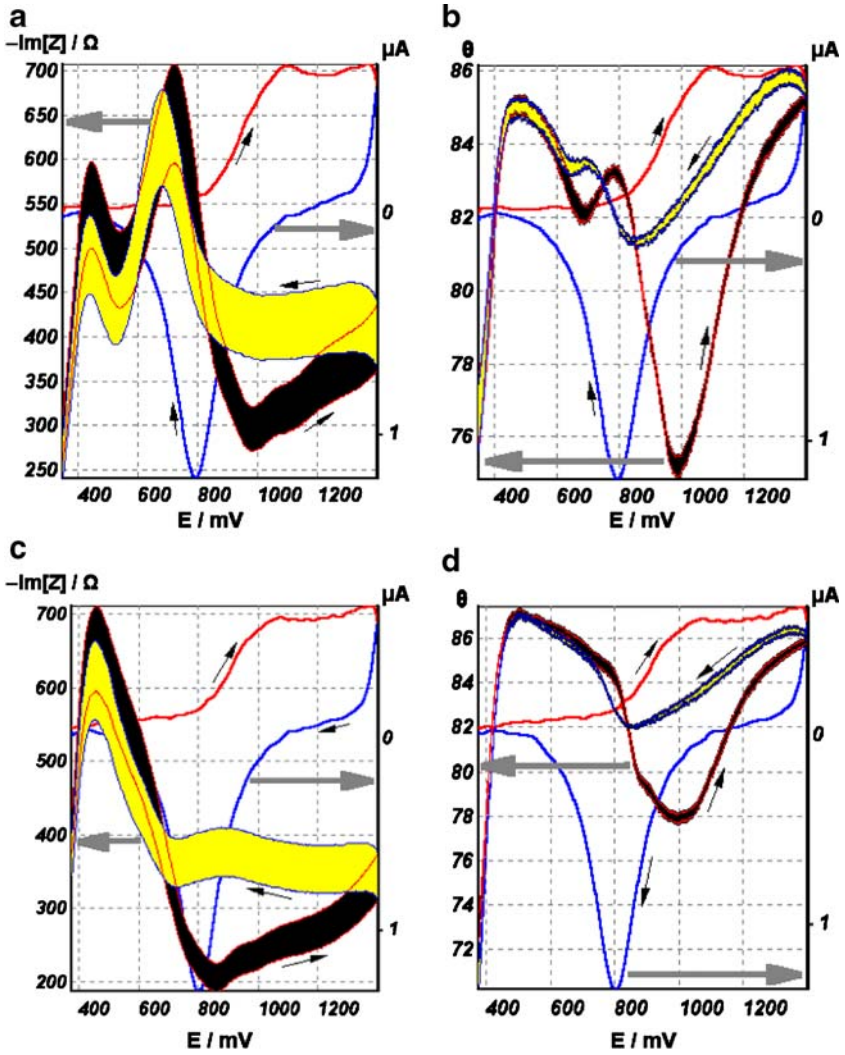

Fig. 4 PDEIS spectra of Pt in 0.5 M H_2SO_4 (**a**, **b**) and 1 M $HClO_4$ (**c**, **d**) at 40 mV/s; same frequencies as in Fig. 3a and b

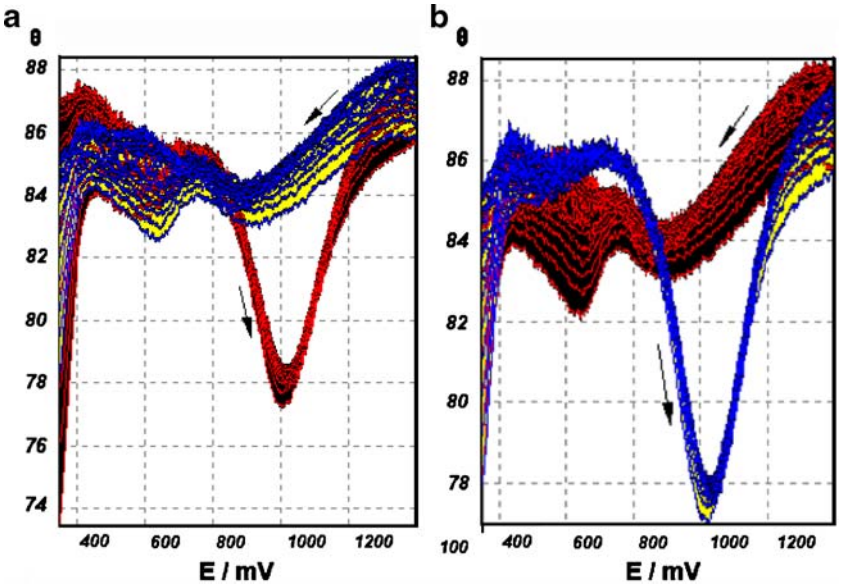

Fig. 5 Phase profiles of the PDEIS spectra of Pt in 0.5 M H_2SO_4 in cyclic scans started from 0.35 V (**a**) and 1.4 V (**b**). d*E*/dt=1.83 mV/s; frequency range, from 23.4 to 439 Hz

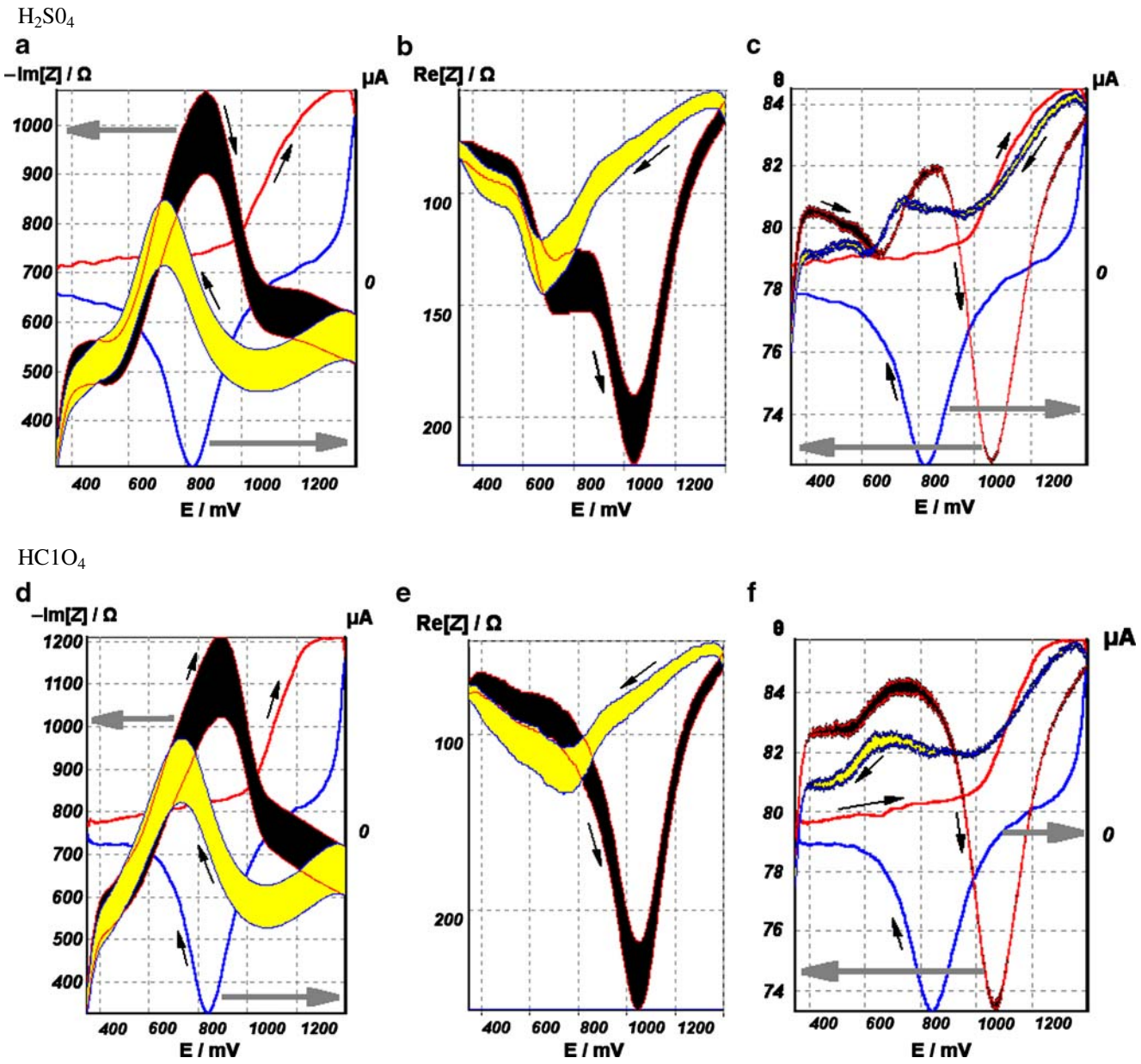

Fig. 6 PDEIS spectra of Pt in 0.5 M H_2SO_4+10^{-4} M KCl (**a**–**c**) and 1 M $HClO_4$+10^{-4} M KCl (**d**–**f**) presented in different coordinate systems and viewed in different perspectives. dE/dt=40 mV/s, f_1=351 Hz, f_2=292 Hz. **a**, **d** Im[Z]=f(*Re*[Z], f, E) viewed along *Re*[Z] axis. **b**, **e** Im[Z]=f(*Re*[Z], f, E) viewed along Im[Z] axis. **c**, **f** $\theta=f(f, E)$ viewed along f-axis

The next section shows how the differences of patterns observed in raw data transform into variations of the parameters of the equivalent circuit.

Dependences of circuit parameters

Equivalent circuit

A general mechanism of Pt anodic oxidation, which accepts a direct oxidation of Pt to PtO, a sequence of two one-electron reactions with $[PtOH]_{ads}$ surface hydroxide formation in the first stage, and also various intermediate cases with fractional charge transfer can be represented by the formal scheme (1, 2):

$$\mathrm{Pt} + \mathrm{H_2O} - z\mathrm{e}^- \underset{k_{-1}}{\overset{k_1}{\rightleftarrows}} [\mathrm{PtOH}_{2-z}]_{\mathrm{ads}} + z\mathrm{H}^+ \quad (1)$$

$$[\mathrm{PtOH}_{2-z}]_{\mathrm{ads}} - (2-z)\mathrm{e}^- \underset{k_{-2}}{\overset{k_2}{\rightleftarrows}} \mathrm{PtO} + (2-z)\mathrm{H}^+ \quad (2)$$

where the first stage (with the forward and backward reaction rate constants k_1 and k_{-1}, correspondingly) is the adsorption with or without the charge transfer ($1 \geq z \geq 0$). At

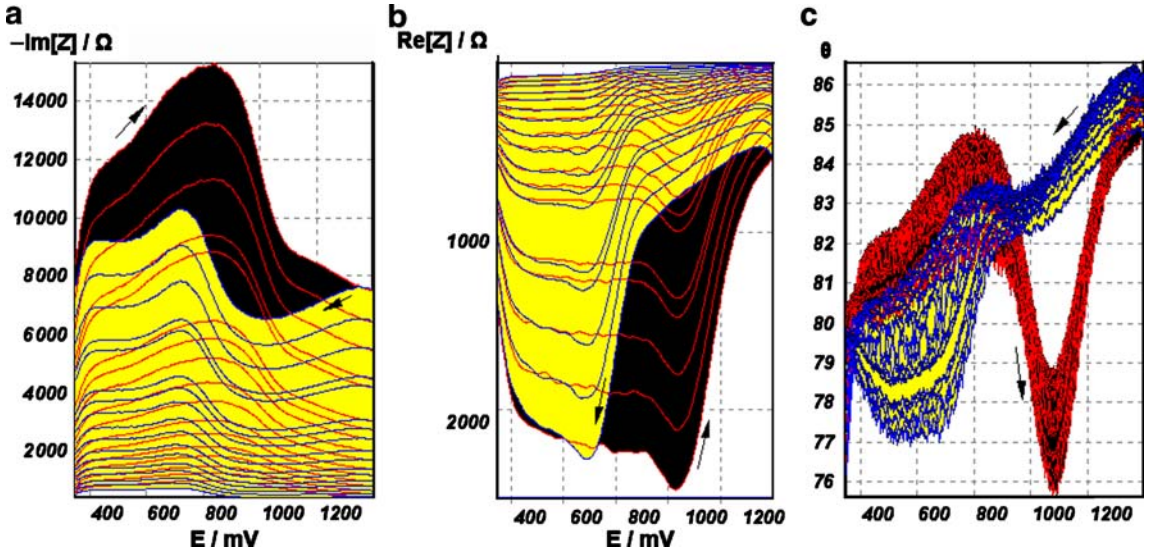

Fig. 7 PDEIS spectra of Pt in 0.5 M H_2SO_4+10^{-4} M KCl. dE/dt=1.83 mV/s; frequency range, from 23.4 to 439 Hz

z=1, this scheme corresponds to a two-stage mechanism of the anodic oxidation of Pt [3]. At z=0, the stage (1) turns to be a physical adsorption of water on Pt, which was considered as the first stage of the direct oxidation of Pt to PtO [6, 7]. Thus, by using the general scheme in the derivation of the equivalent circuit, we reserve the possibility to choose the most appropriate mechanism based on z value.

The net anodic current is the sum of the partial currents due to additivity of the electric charges consumed in the two stages:

$$i = i_1 + i_2. \tag{3}$$

Partial currents i_1 and i_2 related to the stages 1 and 2 are:

$$i_1 = zF \times \left[k_1 C_{H_2O} f_1(\theta_1) - k_{-1} \times C_{H^+}^{z} \times f_{-1}(\theta_1)\right],$$
$$i_2 = (2-z)\mathrm{F} \times \left[k_2 f_2(\theta_1\theta_2) - k_{-2} C_{H^+}^{2-z} \times f_{-2}(\theta_1\theta_2)\right],$$

where $k_1 f_1(\theta_1)$ is the apparent rate coefficient (see, e.g. [45]) of the forward reaction 1 at the bare Pt surface, which depends on the surface coverage θ_1 of $[PtOH_{2-z}]_{ads}$, whilst $k_2 f_2(\theta_1,\theta_2)$ is the apparent rate coefficient of the forward reaction 2, which depends on the surface coverage of both $[PtOH_{2-z}]_{ads}$ and PtO. $f_1(\theta_1)$ and $f_2(\theta_1,\theta_2)$ are the occupancy related factors which are monotonously changing functions of the adsorbate surface coverages θ_1 and θ_2 (e.g. $f_1(\theta_1)=1-\theta_1$ in the case of Langmuir adsorption model).

Faradaic current i is a nonlinear function of the electrode potential E. To derive the Faradaic part of the impedance at a low-amplitude ac perturbation, Eq. 3 is further linearised using the first terms of the Tailor series. With i being the function of E, θ_1 and θ_2, the linearization of Eq. 3 gives:

$$\Delta i = \left(\frac{\partial i}{\partial E}\right)\Delta E + \left(\frac{\partial i}{\partial \theta_1}\right)\Delta\theta_1 + \left(\frac{\partial i}{\partial \theta_2}\right)\Delta\theta_2 \tag{4}$$

where Δi, ΔE, $\Delta\theta_1$ and $\Delta\theta_2$ represent the values which oscillate during the ac probing. To define the functions $\Delta\theta_1$ and $\Delta\theta_2$, we consider the mass balance, similarly to [4]:

$$q_1 \frac{d\Delta\theta_1}{dt} = \Delta(i_1 - i_2) = \Delta r_1 \tag{5}$$

$$q_2 \frac{d\Delta\theta_2}{dt} = \Delta i_2 = \Delta r_2 \tag{6}$$

where q_1 and q_2 are the charges required to form the complete layers of $[PtOH_{2-z}]_{ads}$ and PtO, respectively. Linearisation of the functions Δr_1 and Δr_2 gives:

$$\Delta r_1 = \left(\frac{\partial r_1}{\partial E}\right)\Delta E + \left(\frac{\partial r_1}{\partial \theta_1}\right)\Delta\theta_1 + \left(\frac{\partial r_1}{\partial \theta_2}\right)\Delta\theta_2 \tag{7}$$

$$\Delta r_2 = \left(\frac{\partial r_2}{\partial E}\right)\Delta E + \left(\frac{\partial r_2}{\partial \theta_1}\right)\Delta\theta_1 + \left(\frac{\partial r_2}{\partial \theta_2}\right)\Delta\theta_2 \tag{8}$$

Faradaic admittance $Y(j\omega)=\Delta i/\Delta E$ is obtained by solving Eqs. 4, 7 and 8:

$$Y(j\omega) = A + \frac{B + j\omega D}{j\omega U - \omega^2 + G} \tag{9}$$

where $A=-(\partial i/\partial E)=1/R_{ct}$ is the inverse charge transfer resistance and B, D, U and G are frequency-independent parameters which depend on i, E, θ_1 and θ_2. The Faradaic impedance $Z(j\omega)$ is the inverse of $Y(j\omega)$:

$$Z(j\omega) = R_{ct} + \frac{H + j\omega M}{N + j\omega P + \omega^2 S} = R_{ct} + Z_x(j\omega) \tag{10}$$

Equation 10 corresponds to a series combination of the charge transfer resistance R_{ct} and an additional impedance element Z_x which depends on i, E, θ_1 and θ_2. We have

searched for the equivalent circuit, keeping in mind the Occam's razor principle which states that one should not increase, beyond what is necessary, the number of entities required to explain anything. In the equivalent circuit analysis, this suggests choosing a model which fits to experimental data and contains minimal number of parameters. A CPE appeared to fit well in place of Z_x in the fitting of PDEIS data at early stages of oxide growth and reduction, and C_{dl} was separated from the Faradaic response with perfectly low uncertainty; therefore, we have used an *R*-CPE subcircuit in parallel with C_{dl} in the equivalent circuit shown in Fig. 2.

PDEIS, as a potentiodynamic technique, gives different trajectories for each of the derived parameters in the anodic and cathodic scans. Figure 8 shows the potentiodynamic curves for the double-layer capacitance of Pt electrode in chloride free 0.5 M H_2SO_4, 1 M $HClO_4$ and also with chloride addition in the potential cycles between the lower border of the double-layer region and 1.4 V. In the chloride-free solutions, the C_{dl} depends weakly on the potential in the double-layer region in the anodic scan, increases strongly with the anodic oxidation and decreases with the oxide reduction in the cathodic scan (curve 1 in Fig 8a and curves 1 and 2 in Fig. 8b). A local small maximum of C_{dl} is observed in the double-layer region in the cathodic scan, and this maximum tends to appear even when an anodic scan is reversed at the beginning of Pt oxidation in sulphuric acid (curve 2 in Fig 8a). Thus, the C_{dl} around 20 μF cm^{-2} is the minimal value for platinum in H_2SO_4 in the double-layer region, whilst in platinum oxidation region, the C_{dl} increases more than twice. In $HClO_4$, the situation with the variability of C_{dl} is even more complex. Perchlorate, probably because of much weaker adsorption on Pt than sulphate, poorly stabilises the C_{dl} in the double-layer region, so the value of the minimum in the $C_{dl}(E)$ in the anodic scan is dependent on the previous history of the electrode. This is shown with curves 1 and 2 in Fig. 8b. Curve 1 was obtained after keeping the electrode in the beginning of H upd region, whilst curve 2 was obtained immediately after the scan of curve 1. As the figure shows, the two scans start at different initial capacitances but return to the same values in the reverse scan. The oxide reduction obviously renews the structure of the double layer and thus helps the C_{dl} to behave similarly in the ends of the both scans. By changing the electrode history, the minimum in C_{dl} in perchloric acid in the anodic scan can be easily shifted, and the minimum was found to be in the range between 25 and 35 μF cm^{-2}.

Chloride addition at 10^{-4} M changes the potentiodynamic curves of the double-layer capacitance dramatically (curves 3 in Fig. 8a,b). The effect is especially strong in the case of perchloric acid solution because of higher C_{dl} in the chloride-free solution. In both solutions, the minimum in C_{dl} in the anodic scan shifts in the positive direction and becomes lower. Individual features of sulphate and perchlorate in the C_{dl} variation in Pt oxidation region disappear with chloride addition, so the part of the cycle above 0.8 V looks very similar in perchloric and sulphuric acids with the addition of chloride. However, the C_{dl} behaviour in the double-layer region becomes even more different than in the chloride-free solutions of the two acids. In sulphuric acid, the $C_{dl}(E)$ in this range is not strongly affected by chloride, whilst in the perchloric acid, the C_{dl} dependence on the potential becomes almost linear in the both directions of the scan and shows a strong decrease in C_{dl} with the potential increase.

Figure 9 shows the potentiodynamic curves for the circuit elements which stand in the equivalent circuit in parallel to C_{dl},. All the curves in this figure correspond to the same scans as the curves with the same numbers in Fig. 8b. The parameter R_2 is represented in Fig. 9a by the variation of the inverse value because both the charge transfer resistance of

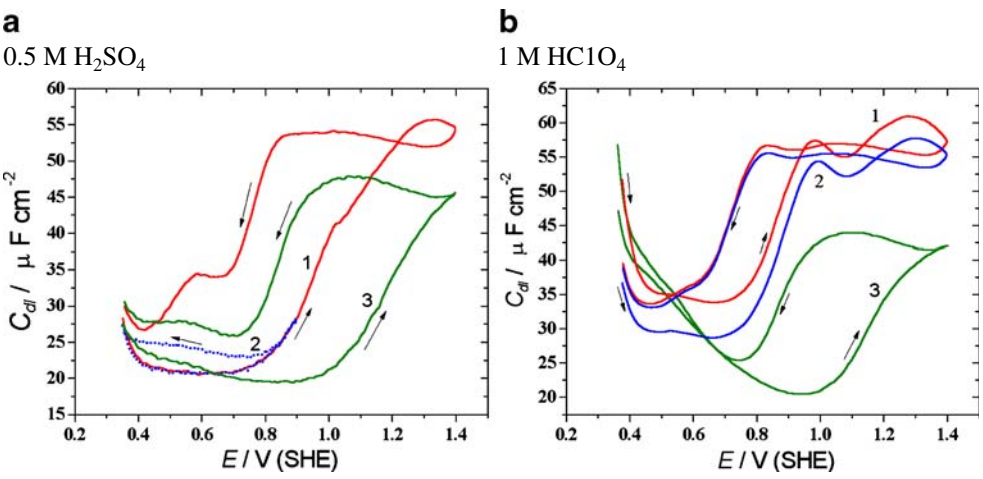

Fig. 8 Double-layer capacitance of Pt electrode variation in cyclic scans at 1.83 mV/s in 0.5 M H_2SO_4 (**a**) and 1 M $HClO_4$ (**b**). Cycle 2 was recorded after cycle 1 (see comments in the text). Curves *3* in **a** and **b** show the effect of 10^{-4} M chloride addition: curve *3* in **a**, 0.5 M H_2SO_4+10^{-4} M KCl; curve *3* in **b**, 1 M $HClO_4$+ 10^{-4} M KCl

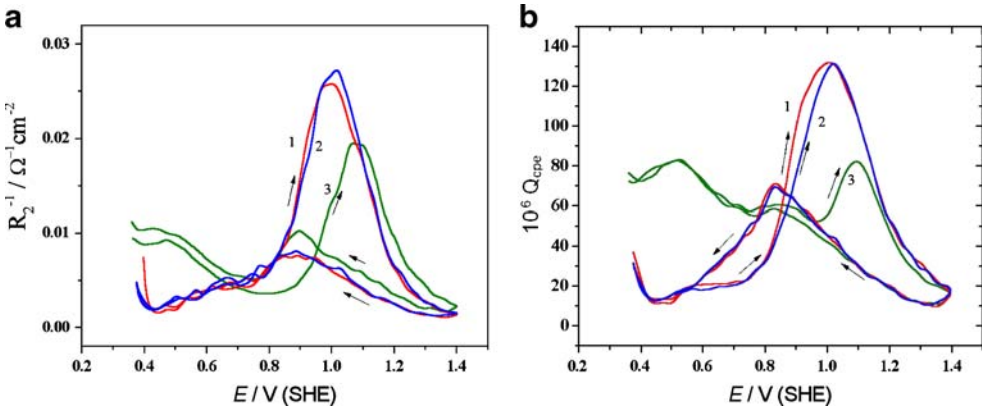

Fig. 9 **a** R_2^{-1} and **b** Q_{cpe} (normalised for surface area) as functions of the potential for platinum in 1 M $HClO_4$ (curves *1*, *2*) and 1 M $HClO_4$+10^{-4} M KCl (curves *3*). Experimental conditions are the same as in Fig. 8b

the electrochemical reaction and the charge transfer resistance that originates in the electrochemical adsorption manifest themselves in the potentiodynamic curves by peaks of inverse values at their corresponding potentials [29]. R_2^{-1} shows the expected peaks in the region of platinum oxidation in the anodic scan and in the region of oxide reduction in the cathodic scan. Chloride addition shifts the anodic peak to higher potential considerably, but has just a small affect on the position of the cathodic peak.

The CPE is the circuit element with the impedance represented by the following formula:

$$Z_{CPE} = Q_{cpe}{}^{-1}(j\omega)^{-n}. \quad (11)$$

The physical meaning of this parameter is rather obscure except the case when the exponent n approaches unity. In that case, Q_{cpe} can be treated as the distorted capacitance. In platinum oxidation, however, the exponent varied around 0.7, almost in the middle between unity, which is a characteristic of capacitor, and 0.5, which is a characteristic of diffusion impedance Z_W:

$$Z_w = A_W(j\omega)^{-0.5}. \quad (12)$$

In this case, Q_{cpe} may be roughly considered as something in between the capacitance and the inverse of the Warburg constant. With this rough interpretation, the peaks in Fig. 9b correspond to enhancement of the ac transmittance resulting from capacitive and diffusion contributions of anodic oxidation and oxide reduction at their corresponding potentials. Probably, the frequency range of our measurements was insufficient to further separate this joint capacitive and diffusional contribution, or the effect of the underlying processes is not reducible to a simple combination of standard circuit elements. Anyway, Fig. 9b gives a clear indication of the shift in the positive direction on the potential scale of the anodic peak, which results from this integral contribution, when chloride is added to perchloric acid solution. The position of the cathodic peak is unaffected by chloride, similarly to the case of $R_2^{-1}(E)$.

The parameters obtained from the frequency response analysis provide a more detailed description of the object. In particular, the anodic charge in platinum oxidation can be calculated taking into account the information on the variability of the charging current which results from the variation of the double-layer capacitance in the anodic scan. A substantial increase in the double-layer capacitance in the anodic scan results in the consumption of a sensible part of the total current for the double-layer charging. Figure 10 shows the anodic charges of Pt in 0.5 M H_2SO_4 and 1 M $HClO_4$ as functions of the potential calculated

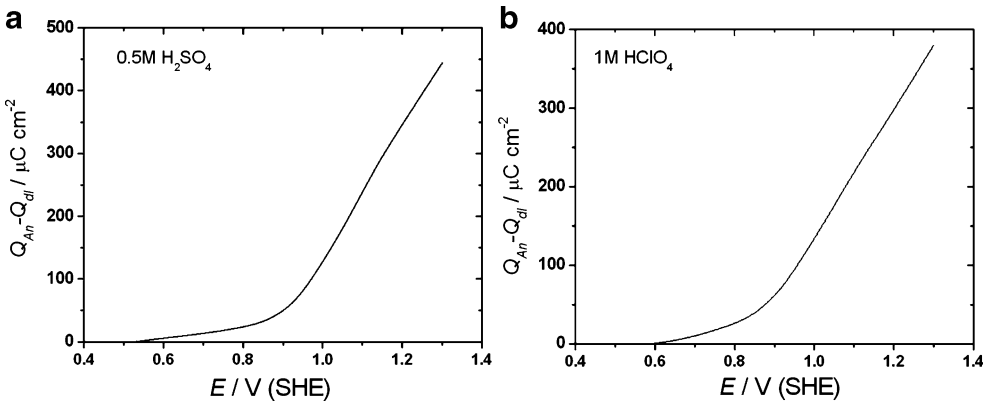

Fig. 10 Anodic charge of platinum in the anodic scan calculated from Fig. 1a (**a**) and b (**b**) and corrected for the variable double-layer capacitance

with the charging current correction based on the double-layer profiles obtained with PDEIS. The data, which are needed for the joint analysis of the ac and dc response of this kind, in principle, can be obtained in a single scan by correcting the dc part of the response with the charging current obtained from equivalent circuit analysis of the ac part of the response, and this is probably one of the directions for the future electroanalytical techniques to make efficient combinations of ac and dc signal processing within single experiment and single routine.

To secure the double-layer capacitance separation from the parallel *R*-CPE branch, we have checked also more general models with the double layer represented by CPE; however, the CPE in parallel with the Faradaic branch always reduced in the fitting to a pure capacitor (*n* factor approached unity), and the generalisation in the presentation of the double-layer part of ac response did not effect the C_{dl} separation from the parallel branch. The strong potential dependence of the capacitance proves to be a property of the double layer on platinum, not an admixture of a Faradaic response.

There may be different reasons for the C_{dl} dependence on E in the double layer and Pt redox regions. Recent optical investigations of double layer on platinum in $HClO_4$ with sum frequency generation [46] have disclosed reorientation of water molecules in the double-layer region with the electrode potential increase. The transition to "oxygen down" orientation of H_2O molecules favours formation of a more compact double layer, and this may be a reason of the C_{dl} increase before the anodic oxidation starts. Molecules of water are normally linked by hydrogen bonds into a loose network, and some of these bonds should be broken or reorganised when the interfacial layer changes its orientation. The reorientation in the interfacial layer should be slow and irreversible because of the steric factor, and this can cause the hysteresis in C_{dl} variation (even in perchloric acid, which interacts weakly with platinum, the hysteresis was strong in absence of chloride—see Fig. 8b). Further in the anodic scan, the nature of the double layer changes with the anodic oxidation of Pt. Oxidised platinum group metals are known supercapacitor materials, so the high value of C_{dl} in the oxidised state on Pt could be expected. The similar rise in C_{dl} at the end of the double-layer region and at the beginning of Pt anodic oxidation gives a hint that the interaction of oxygen atoms of the adsorbed water with Pt surface continues to affect the C_{dl} at the initial stage of anodic oxidation. An ordered layer of hydroxyl groups or oxygen atoms can obviously form a more effective plate of a capacitor than a loose layer of ions incorporated in a network of water molecules. The levelling effect of chloride in the C_{dl} variation is evidently due to its adsorption on Pt.

The major part of Faradaic admittance of Pt interfaces with sulphuric and perchloric acids falls to the potential region of redox transformations (Fig. 9). The R_2 dependence on E in Pt redox region is a useful source of information about kinetics of platinum oxidation and reduction, and the application of this possibility will be considered in a separate publication. A sensible contribution to the admittance from the Faradaic branch in the double-layer region, similarly to C_{dl} variation, can originate in the network of water molecules restructuring in the interfacial layer. The restructuring of the adsorbed water has some similarity both with electrochemical adsorption and diffusion. Pure electrochemical adsorption would give RC contribution with $n=1$ in $(j\omega)^{-n}$ term of the impedance, whilst a reaction with diffusion would give RW contribution with $n=0.5$ in the similar term of impedance. Therefore, it is quite natural that an *R*-CPE subcircuit with intermediate values of the exponent approximates this effect. Because of small contribution of the Faradaic branch, its detailed analysis is presently unavailable in the double-layer region.

Conclusions

Potentiodynamic electrochemical impedance spectroscopy has enabled monitoring of the variable interface between Pt and a solution of perchloric or sulphuric acid by obtaining separate potentiodynamic curves for the double-layer capacitance and two elements in the Faradaic branch of equivalent circuit—charge transfer resistance and a constant phase element. Platinum anodic oxidation modifies the chemical nature of the interfacial layer, and this is manifested by strong increase in C_{dl} and also by peaks of inverse charge transfer resistance and constant phase element. The double-layer capacitance has been shown to increase more than twice in the anodic scan from the double-layer region to the region of platinum oxide growth. Potentiodynamic curves of raw data were also informative, especially the phase shift, which showed a pronounced minimum in Pt anodic oxidation region and a smaller minimum in the cathodic scan in the region of platinum oxide reduction. Both the raw potentiodynamic curves and the variation of equivalent circuit parameters obtained from PDEIS spectra analysis extend considerably the informativeness of the potentiodynamic approach of the electrochemical interface characterisation.

Acknowledgements Fuel Cell Laboratory of the Nissan Research Center is kindly acknowledged for support of this work in B-1565p project of the International Science and Technology Center.

References

1. Butler JAV, Pearson R (1938) Trans Faraday Soc 34:1163. doi:10.1039/tf9383401163
2. Burke LD (1986) In: Bockris JO'M, White RE, Conway BE (eds) Modem aspects of electrochemistry, vol 18, Chapter 4. Plenum, New York
3. Conway BE (1995) Prog Surf Sci 49:331. doi:10.1016/0079-6816(95)00040-6
4. Harrington DA (1997) J Electroanal Chem 420:101. doi:10.1016/S0022-0728(96)04813-9
5. Sun A, Franc J, MacDonald DD (2006) J Electrochem Soc 153:B260. doi:10.1149/1.2200156
6. Jerkiewicz G, Vatankhah G, Lessard J, Soriaga MP, Park Y-S (2004) Electrochim Acta 49:1451
7. Alsabet M, Grden M, Jerkiewicz G (2006) J Electroanal Chem 589:120. doi:10.1016/j.jelechem.2006.01.022
8. Juodkazis K, Juodkazytė J, Juodienė T, Šukienė V, Savickaja I (2006) Electrochim Acta 51:6159. doi:10.1016/j.electacta.2006.01.071
9. Berná A, Climent V, Feliu JM (2007) Electrochem Commun 9:2789
10. Garcia-Araez N, Climent V, Feliu JM (2008) J Solid State Electrochem 12:387. doi:10.1007/s10008-007-0417-y
11. Jacob T (2007) J Electroanal Chem 607:158. doi:10.1016/j.jelechem.2007.03.023
12. Teliska M, O'Grady WE, Ramaker DE (2005) J Phys Chem B 109:8076. doi:10.1021/jp0502003
13. Viswanath RN, Kramer D, Weissmüller J (2008) Electrochim Acta 53:2757. doi:10.1016/j.electacta.2007.10.049
14. Makharia R, Kocha S, Yu PT, Sweikart MA, Gu W, Wagner FT et al (2006) ECS Trans 1(8):3. doi:10.1149/1.2214540
15. Borup R, Meyers J, Pivovar B, Kim YS, Mukundan R, Garland N et al (2007) Chem Rev 107:3904. doi:10.1021/cr0501821
16. Uchimura M, Kocha S (2007) ECS Trans. 11(1):1215. doi:10.1149/1.2781035
17. Shao Y, Yin G, Gao Y (2007) J Power Sources 171:558. doi:10.1016/j.jpowsour.2007.07.004
18. Wang X, Kumar R, Myers DJ (2006) Electrochem Solid-State Lett 9:A225. doi:10.1149/1.2180536
19. Shao-Horn Y, Sheng WC, Chen S, Ferreira PJ, Holby EF, Morgan D (2007) Top Catal 46:285. doi:10.1007/s11244-007-9000-0
20. Bi W, Fuller TF (2008) J Power Sources 178:188. doi:10.1016/j.jpowsour.2007.12.007
21. Łukaszewski M, Czerwiński A (2006) J Electroanal Chem 589:38. doi:10.1016/j.jelechem.2006.01.007
22. Yadav AP, Nishikata A, Tsuru T (2007) Electrochim Acta 52:7444. doi:10.1016/j.electacta.2007.06.029
23. Funtikov AM, Stimming U, Vogel RJ (1997) Electroanal Chem 428:147. doi:10.1016/S0022-0728(96)05051-6
24. Thomas S, Sung YE, Kim HS, Wieckowski A (1996) J Phys Chem 100:11726. doi:10.1021/jp9606321
25. Pajkossy T, Kolb DM (2001) Electrochim Acta 46:3063–3071. doi:10.1016/S0013-4686(01)00597-7
26. Pajkossy T, Kolb DM (2007) Electrochem Commun 9:1171. doi:10.1016/j.elecom.2007.01.002
27. Pell WG, Zolfaghari A, Conway BE (2002) J Electroanal Chem 532:13. doi:10.1016/S0022-0728(02)00676-9
28. Marian E, van der Geest ME, Dangerfield NJ, Harrington DA (1997) J Electroanal Chem 420:89. doi:10.1016/S0022-0728(96)04812-7
29. Ragoisha GA, Bondarenko AS (2005) Electrochim Acta 50:1553. doi:10.1016/j.electacta.2004.10.055
30. Ragoisha GA, Bondarenko AS (2005) In: Nunez M (ed) Electrochemistry: new research. Nova Science, New York
31. Ragoisha GA, Bondarenko AS (2003) Solid State Phenom 90-91:103
32. Bondarenko AS, Ragoisha GA (2005) J Solid State Electrochem 9:845. doi:10.1007/s10008-005-0025-7
33. Ragoisha GA (2004-2008) Potentiodynamic Electrochemical Impedance Spectroscopy web pages.. doi:http://www.abc.chemistry.bsu.by/vi/
34. Schiewe J, Hazi J, Vicente-Beckett VA, Bond AM (1998) J Electroanal Chem 451:129. doi:10.1016/S0022-0728(97)00579-2
35. Ragoisha GA, Bondarenko AS (2003) Electrochem Commun 5:392. doi:10.1016/S1388-2481(03)00075-4
36. Ragoisha GA, Bondarenko AS, Osipovich NP, Streltsov EA (2004) J Electroanal Chem 565:227. doi:10.1016/j.jelechem.2003.10.014
37. Bondarenko AS, Ragoisha GA, Osipovich NP, Streltsov EA (2005) Electrochem Commun 7:631. doi:10.1016/j.elecom.2005.04.001
38. Ragoisha GA, Bondarenko AS, Osipovich NP, Rabchynski SM, Streltsov EA (2008) Electrochim Acta 53:3879. doi:10.1016/j.electacta.2007.09.017
39. Bondarenko AS, Ragoisha GA, Osipovich NP, Streltsov EA (2006) Electrochem Commun 8:921. doi:10.1016/j.elecom.2006.03.033
40. Trasatti S, Petrii OA (1992) J Electroanal Chem 327:353. doi:10.1016/0022-0728(92)80162-W
41. Bondarenko AS, Ragoisha GA (2005) In: Pomerantsev AL (ed) Progress in chemometrics research. Nova Science, New York
42. Bondarenko AS, Ragoisha GA (2007) EIS spectrum analyzer.. doi:http://www.abc.chemistry.bsu.by/vi/analyser/
43. Garland JE, Pettit CM, Roy D (2004) Electrochim Acta 49:2623. doi:10.1016/j.electacta.2003.12.051
44. Sibert E, Faure R, Durand R (2001) Electrochem Commun 3:181. doi:10.1016/S1388-2481(01)00130-8
45. Kerner Z, Pajkossy T (2002) Electrochim Acta 47:2055. doi:10.1016/S0013-4686(02)00073-7
46. Noguchi H, Okada T, Uosaki K (2008) Electrochim Acta 53:6841. doi:10.1016/j.electacta.2008.02.094